Inorganic Chemistry

pubs.acs.org/IC

Article

Extensive Redox Non-Innocence in Iron Bipyridine-Diimine Complexes: a Combined Spectroscopic and Computational Study

Ranjeesh Thenarukandiyil, Eno Paenurk, Anthony Wong, Natalia Fridman, Amir Karton, Raanan Carmieli, Gabriel Ménard, Renana Gershoni-Poranne,* and Graham de Ruiter*

Cite This: *Inorg. Chem.* 2021, 60, 18296−18306

Read Online

ACCESS | Metrics & More | Article Recommendations | Supporting Information

ABSTRACT: Metal−ligand cooperation is an important aspect in earth-abundant metal catalysis. Utilizing ligands as electron reservoirs to supplement the redox chemistry of the metal has resulted in many new exciting discoveries. Here, we demonstrate that iron bipyridine-diimine (BDI) complexes exhibit an extensive electron-transfer series that spans a total of five oxidation states, ranging from the trication $[Fe(BDI)]^{3+}$ to the monoanion $[Fe(BDI]^{-1}$. Structural characterization by X-ray crystallography revealed the multifaceted redox noninnocence of the BDI ligand, while spectroscopic (e.g., ^{57}Fe Mössbauer and EPR spectroscopy) and computational studies were employed to elucidate the electronic structure of the isolated complexes, which are further discussed in this report.

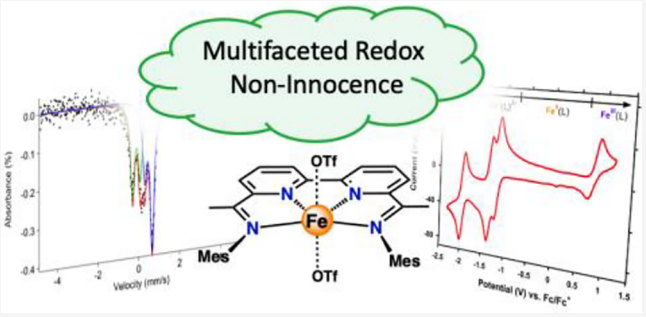

INTRODUCTION

Over the past decade, metal−ligand cooperativity has established itself as a valuable asset in catalysis.[1] The ability of a ligand to participate in proton transfer,[2] electron transfer,[3] and bond-activation processes[4] has revealed unparalleled reactivity pathways that were previously unexplored. In particular, the participation of the ligand in useful redox events is an important feature used by metallo-enzymes to catalyze essential chemical and biological transformations.[5] Besides their importance in biology, the application of redox noninnocent ligands in catalysis has recently shifted the paradigm that mainly noble metals can participate in reversible two-electron chemistry.[6] Furthermore, Wieghardt and Chirik have recently emphasized that noble metal reactivity can be conferred upon the first-row transition metals by clever ligand design.[7]

The realization that ligands can participate in redox processes was recognized in the early 1960s by Gray and co-workers.[8] Since then, many redox-active ligands have been developed that typically feature electron-donating or π-accepting systems capable of stabilizing radical cations and/or anions.[6a−d] Typical examples include (i) 1,2-substituted semibenzoquinone based architectures[8a,9] or (ii) those that contain α-imino substituents.[10] In particular, redox non-innocent pyridinediimine based ligands (Figure 1) have gained significant interest as their iron,[11] cobalt,[12] nickel,[13] and manganese[14] complexes have proven to be active catalysts in a variety of transformations.[15]

Their reactivity is partially attributed to the rich electrochemistry resulting from an interplay between the redox-activity of the ligand[16] and the metal.[10b,17] In these complexes, the observed electron transfer is usually between one and three electrons, whereas multiple electron transfers >3 are uncommon.[18]

Here, we present an iron complex of the type $[Fe(BDI)(OTf)_2]$ (**2**; BDI = bipyridine-diimine, Figure 1), whose electron-transfer series spans five distinct oxidation states. The ability to isolate each species enabled us to show the electronic metal−ligand cooperativity, in which both the ligand (BDI ⇄ BDI^{3-}) and the metal (M^{II} ⇄ M^{III}) have distinctive roles. Specifically, crystallographic, spectroscopic, and computational studies provided insight into the electronic structure of these complexes and how the consecutive one-electron reductions lead to the formation of a ligand-based trianion, which is further discussed in this study.

RESULTS AND DISCUSSION

Intrigued by the reactivity[19] and electronic structure[20] of the pyridinediimine (PDI) complexes, we prepared a series of iron−metal complexes based on bipyridine (Figure 2A). It was

Received: September 19, 2021
Published: November 17, 2021

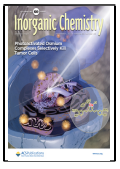

ACS Publications

© 2021 American Chemical Society

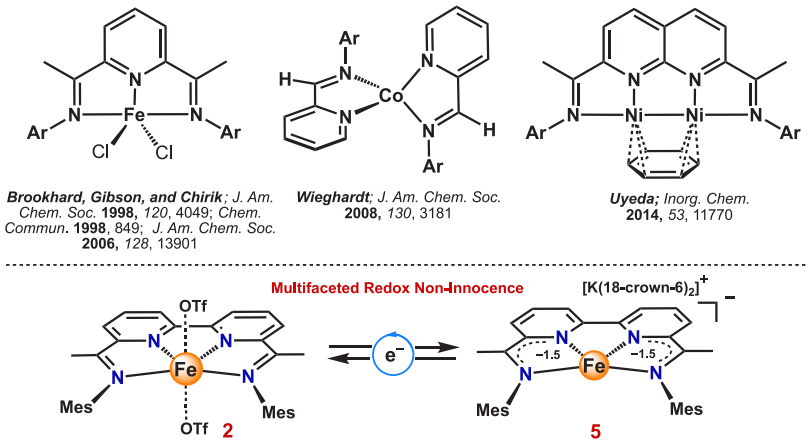

Figure 1. (Top) Representative examples of previously reported redox-active ligands containing aryl-substituted (bis)-iminopyridine-based backbones. (Bottom) Herein reported redox noninnocence of aryl-substituted bis-iminobipyridine-based iron complexes.

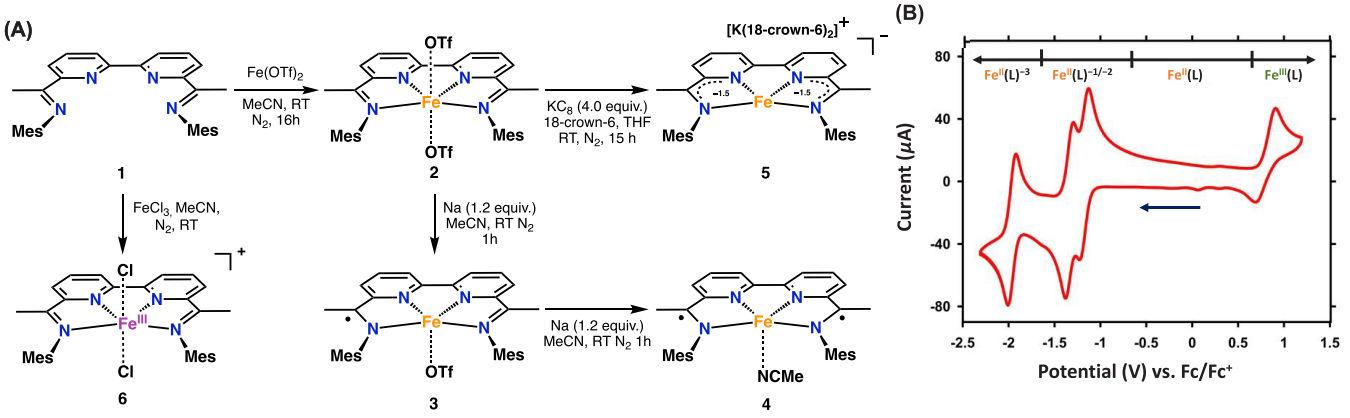

Figure 2. (A) Synthesis of complexes **2**–**6**. (B) Cyclic voltammogram (CV) of **2** recorded at a scan rate of 200 mV s^{-1} in acetonitrile (2 mM) with 0.1 M [^{n}Bu$_4$N][PF$_6$] as a supporting electrolyte. The arrow indicates the scanning direction.

previously demonstrated that earth-abundant metal complexes with bipyridine or phenanthroline ligands are outstanding catalysts in a variety of organic transformations.[21] Realizing that bipyridine is (i) an excellent ligand toward first-row transition metals[22] and (ii) redox-active at negative potentials,[23] we reasoned that incorporating *ortho*-imino substituents into a bipyridine platform could potentially lead to increased stability of the resulting metal complexes, while simultaneously enabling multielectron transfer that is primarily ligand-based. Although Solan and co-workers have reported on structurally related complexes,[24] the observed solid- and solution-state flexibility might have prevented further investigations into those systems' electronic and catalytic properties.[24]

Synthesis of Iron Complexes. To initiate our studies, we prepared complex [Fe(BDI)(OTf)$_2$] (**2**) by stirring an acetonitrile solution of BDI and anhydrous Fe(OTf)$_2$ at RT for 16 h. The ^{1}H NMR spectrum of **2** showed well-defined, paramagnetically shifted resonances in the range between −30 and 50 ppm, consistent with the presence of a single monometallic species of higher symmetry (Figure S4). Analysis of aliquots of the reaction mixture by electrospray ionization mass spectrometry revealed a peak at m/z = 679.17, consistent with the formation of [Fe(BDI)][OTf]$^+$ (Figure S5). Crystals suitable for X-ray crystallography were obtained by slow vapor diffusion of diethyl ether into a concentrated solution of **2** in tetrahydrofuran (Figure 3). Iron complex **2** crystallizes in a distorted octahedral geometry with two triflates occupying the

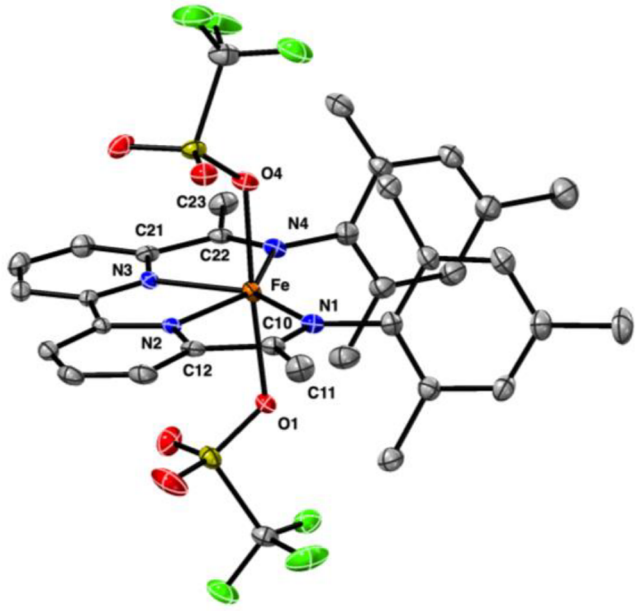

Figure 3. Solid-state structure of [Fe(BDI)(OTf)$_2$] (**2**). Thermal ellipsoids are shown at the 30% probability level. Hydrogen atoms and cocrystallized solvent molecules are omitted for clarity. See Tables 1 and S3 for selected bond angles and distances.

https://doi.org/10.1021/acs.inorgchem.1c02925
Inorg. Chem. 2021, 60, 18296−18306

Table 1. Selected Experimental and Calculated Bond Distances (in Å) for Complexes 2−5[a]

	[Fe(BDI)(OTf)$_2$] (**2**)[b]		[Fe(BDI)(OTf)] (**3**)[b]		[Fe(BDI)(MeCN)] (**4**)[b]		[Fe(BDI)][K(18-crown-6)$_2$] (**5**)[b]	
	exptl.	calcd. (quintet)	exptl.	calcd. (BS 2.1)	exptl.	calcd. (BS 2.2)	exptl.	calcd. (BS 2.1)
Fe−N1	2.252(2)	2.172	1.999(7)	2.028	1.965(2)	1.978	1.920(3)	1.943
Fe−N2	2.128(2)	2.127	1.842(7)	1.865	1.848(2)	1.860	1.828(2)	1.848
Fe−N3	2.132(3)	2.131	1.854(8)	1.859	1.841(2)	1.858	1.832(3)	1.849
Fe−N4	2.229(2)	2.168	1.98(1)	1.971	1.952(2)	1.976	1.925(2)	1.941
N1−C10	1.276(4)	1.277	1.32(1)	1.302	1.352(3)	1.342	1.383(3)	1.372
C10−C12	1.490(5)	1.488	1.41(1)	1.452	1.419(3)	1.417	1.387(5)	1.389
C12−N2	1.345(4)	1.325	1.37(1)	1.343	1.372(3)	1.363	1.407(5)	1.384
N4−C22	1.276(4)	1.276	1.32(1)	1.325	1.343(3)	1.336	1.378(5)	1.372
C22−C21	1.490(5)	1.488	1.43(2)	1.428	1.418(4)	1.420	1.401(5)	1.389
N3−C21	1.347(4)	1.324	1.35(1)	1.359	1.372(3)	1.365	1.399(5)	1.385

[a]For a numbering scheme, see Figure 1 or Figure S14. [b]Calculations were performed with the PBE0 functional and def2-TZVP basis set, using Grimme's D3 dispersion correction with Becke−Johnson damping (see Supporting Information and Computational Methods for more details).

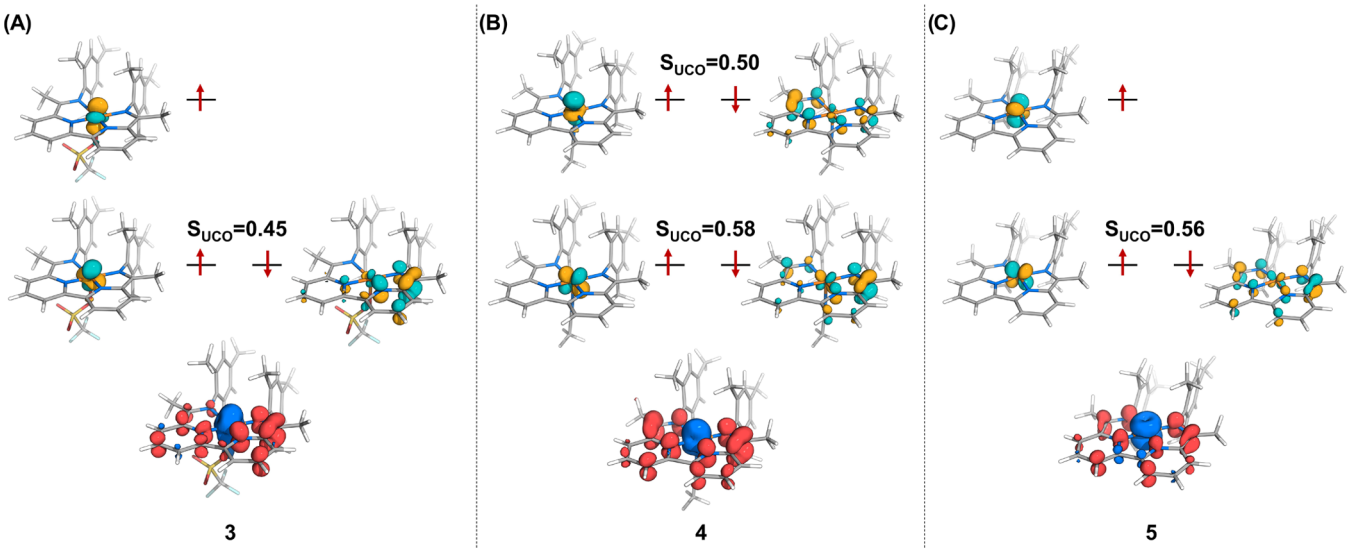

Figure 4. Partial molecular orbital energy diagrams (top) and total spin−density plot (bottom) for (A) [Fe(BDI)(OTf)] (**3**), (B) [Fe(BDI)(MeCN)] (**4**), and (C) [Fe(BDI)][K(18-crown-6)$_2$] (**5**). The orbitals shown are the unrestricted corresponding orbitals; the values reported are the overlaps between the antiferromagnetically coupled orbitals. Positive spin−density is shown in blue, and negative spin−density is shown in red.

axial positions. On the basis of charge balance, the iron metal center is assigned as Fe^{II}, which is further corroborated by the average $C_{imine}-N_{imine}$ and $C_{ipso}-C_{imine}$ distances of 1.276 and 1.490 Å, respectively, indicating a neutral BDI ligand (Table 1).[10b−d] Summaries of relevant bond distances and angles are given in Tables 1 and S3, respectively. Computed bond lengths for the quintet ground state (Table 1) show good agreement with the experimental values, and localized orbital bonding analysis (LOBA)[25] calculations corroborated a +2 oxidation state for Fe (see Computational Methods and Supporting Information for further details).

Interestingly, crystallizing the iron complex from acetonitrile yielded a pentagonal bipyramidal geometry with an equatorially coordinated acetonitrile molecule (**7**; Figure S20). The presence of this acetonitrile molecule leads to elongation of the mesityl centroid−centroid distances from 5.595 Å in **2** to 6.241 Å in **7** (Figure S20, Table S3). The structural flexibility of the coordination geometry can have important implications in catalytic transformations, where the availability of both an axial and an equatorial coordination site is important (e.g., for oxidative addition and reductive elimination).

Electrochemical Studies. Having established the solid-state structure of **2**, its redox properties were investigated by cyclic voltammetry. The cyclic voltammogram (CV) of **2** (Figure 2B; red trace) features three reversible redox waves at $E_{1/2}$ = −1.17, −1.33, and −1.96 V, referenced to the ferrocene/ferrocenium (Fc/Fc^+) redox couple. On the basis of literature data,[10f] all the reductive redox waves are assigned to three consecutive one-electron reductions of the neutral $[BDI]^0$ ligand to the radical trianion $[BDI]^{3-}$.[16] In addition to these reductive redox waves, complex **2** also exhibits an additional quasi-reversible oxidative feature at $E_{1/2}$ = 0.80 V that suggests a metal-based oxidation from Fe^{II} to Fe^{III}. While we have not been able to isolate this oxidized species, a related Fe^{III} complex $[Fe^{III}(BDI)(Cl)_2]^+$ (**6**) was prepared independently. The CV of **6** shows mainly irreversible oxidation/reduction events, indicating that such an Fe^{III} species might be unstable under electrochemical conditions (Figure S13). Nonetheless, these electrochemical data indicate an extensive electron transfer series, where both the redox-activity of the ligand (i.e., $[BDI]^0 \rightleftarrows [BDI]^{3-}$), as well as that of the metal (i.e., $M^{II} \rightleftarrows M^{III}$), give rise to a total of five different oxidation states (Figure 2A).

https://doi.org/10.1021/acs.inorgchem.1c02925
Inorg. Chem. 2021, 60, 18296−18306

A literature survey shows that metal complexes that can exist in five or more oxidation states are uncommon. Most notable examples include (i) tris-bipyridine or phenanthroline (NN) metal complexes of the type $[M(NN)_3]^n$ ($n = 4^+$ to 3^-),[26] (ii) metal dithiolene (DT) complexes of the type $[(M(DT)_3]^n$ ($n = 1^+ - 4^-$),[27] (iii) iron nitrosyl dithiolene (DT) complexes of the type $[Fe(NO)(DT)_2]^n$ ($n = 1^+ - 3^-$),[28] and (iv) porphyrin analogs,[29] among others.[18,30] In most of these examples, the metal complex contains more than one redox-active ligand, while complexes containing a single redox-active ligand generally exhibit fewer oxidation states.[31]

Characterization and Electronic Structure of Reduced Iron Complexes. As evident from the electrochemical experiments, iron complex **2** can accept a total of three additional electrons (Figure 2B). To evaluate the extent of ligand participation in these reduction events, we used spectroscopic and crystallographic methods together with broken symmetry calculations in order to evaluate the redox noninnocence of the ligand in more detail (Figure 4; see Computational Methods and Supporting Information for further details).

We begin by noting that for iron complex **2**, there is a good agreement between the bond metrics of the solid-state structure and the DFT-optimized structure (Table 1). The mean absolute deviation (MAD) of the calculated and experimentally obtained N−Fe bond lengths for **2** is 0.036 Å, while for the remaining bond distances detailed in Table 1, the MADs are even smaller (0.008 Å).

The agreement between the calculated and experimental bond distances is important as Wieghardt and Chirik have shown that the values for the $C_{imine}-N_{imine}$ and $C_{ipso}-C_{imine}$ bond distances are indicative of the charge state of the ligand.[10b−d] Consequently, the experimentally determined $C_{imine}-N_{imine}$ and $C_{ipso}-C_{imine}$ bond distances of 1.276 and 1.490 Å indicate a neutral BDI ligand, coordinated to a high-spin ($S = 2$) iron(II) metal center (Table 1). DFT calculations agree with such a high-spin ($S = 2$) assignment in complex **2**, where four unpaired electrons are in essentially metal-based orbitals, which is evident from the Löwdin spin population (3.74) on iron. These data are also consistent with the room temperature magnetic moment (SQUID; $\mu_{eff} = 5.24$) and the obtained zero-field ^{57}Fe Mössbauer spectrum of **2**, which shows a single quadrupole doublet with an isomer shift (δ) of 0.67 mm/s and a quadrupole splitting ($|\Delta E_Q|$) of 1.12 mm/s (Figure 5).

According to the CV of **2**, a one-electron reduced species should be accessible at $E_{1/2} = -1.17$ V (vs Fc/Fc^+). Indeed, the addition of 1 equiv of Na(Hg) to a solution of **2** in acetonitrile resulted in the formation of a new species (**3**) as judged by X-ray crystallography (Figure 6A). The solid-state structure of **3** features an iron metal center in a square-pyramidal geometry with a single triflate anion at the axial position, consistent with a one-electron reduction process.

Analysis of the bond metrics revealed that the $N_{imine}-C_{imine}$ bond distances elongate from 1.275(4) Å in **2** to 1.31(1) Å in **3**, while the $C_{imine}-C_{ipso}$ bond distances contract from 1.490(5) Å in **2** to 1.42(1) Å in **3** (Table 1). These changes are suggestive of a ligand-based reduction, which served as the basis for the broken symmetry calculations.

In order to obtain an accurate description of the electronic structure of **3**, we calculated single-point energies for several different electronic configurations using the crystal structure coordinates of complex **3**. More specifically the doublet, quartet, and the BS(4,1), and BS(2,1) electronic configurations were evaluated, which result from a metal or ligand based reduction and iron in a low-spin, high-spin, or intermediate-spin configuration (see Supporting Information for more details). Of these configurations, the BS(2,1) was determined to be the best electronic description of the system (Table S5) and, as a result, was used for the full optimization of the structure. As evident from Table 1, the bond metrics obtained from the BS(2,1) solution are in excellent agreement with those obtained from X-ray crystallography. Overall, these DFT studies suggest an intermediate spin ($S = 1$) iron(II) metal center that is antiferromagnetically coupled to an $S = 1/2$ ligand-based radical, giving an overall doublet spin state for iron complex **3**.

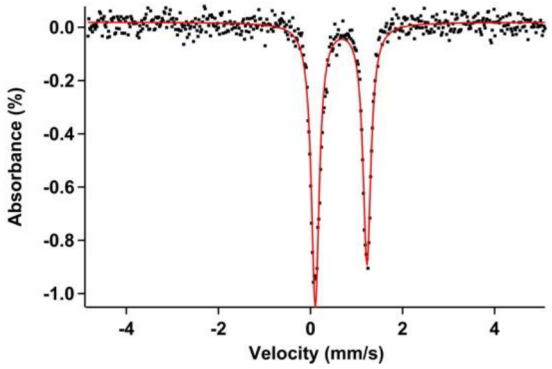

Figure 5. Zero-field ^{57}Fe Mössbauer spectrum (90 K) of [Fe(BDI)-$(OTF)_2$] (**2**) showing a single quadrupole doublet with an isomer shift (δ) value of 0.67 mm/s and quadrupole splitting ($|\Delta EQ|$) value of 1.12 mm/s.

The overall doublet spin state was also confirmed by EPR spectroscopy via transient nutation experiments, which is an excellent technique to determine the overall spin-state of molecular systems (see Supporting Information for more experimental details).[32] The Fourier transform of the nutation experiment of **3** is shown in Figure 6B along with that of a known radical $S = 1/2$ species (i.e., α,γ-bis-diphenylene-β-phenylallyl; BDPA). The near-unity of the ratio between the nutation frequency of **3** and that of the stable radical BDPA indicates an overall doublet spin state, which is consistent with a ligand-based radical ($S = 1/2$) that is antiferromagnetically coupled to an intermediate spin ($S = 1$) iron metal center. Furthermore, the X-band EPR spectrum of **3** in frozen acetonitrile solution reveals a weak signal at 3324 G (Figure 6C; $g = 2.098$), indicative of radical character on the ligand.

To further investigate the validity of the suggested BS(2,1) state, we recorded the zero-field ^{57}Fe Mössbauer spectrum of **3** at 90 K (Figure 6D). The experimentally determined Mössbauer parameters for the major species (82%; $\delta = 0.30$ mm/s; $|\Delta E_Q| = 1.16$ mm/s) agree reasonably well with the calculated values ($\delta = 0.32$ mm/s; $|\Delta E_Q| = 1.87$ mm/s). These values are also consistent with the presence of an intermediate spin ($S = 1$) iron(II) metal center.[10b,33] Overall, the experimental data obtained by X-ray crystallography, EPR spectroscopy, and Mössbauer spectroscopy are in agreement with the computational BS(2,1) solution.

Because the computational and experimental data are in good agreement, we calculated the partial molecular orbital energy diagram of complex **3** (Figure 4A). As evident from Figure 4A, the two unpaired spin-up electrons are essentially located in metal-based orbitals, whereas the spin-down

https://doi.org/10.1021/acs.inorgchem.1c02925
Inorg. Chem. 2021, 60, 18296−18306

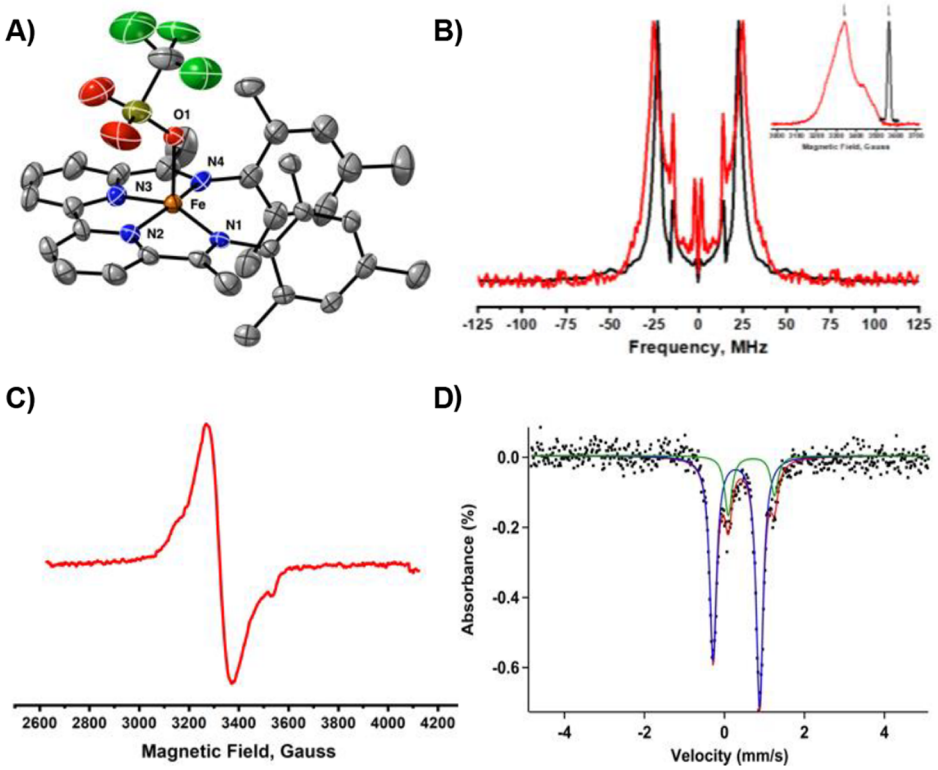

Figure 6. (A) Solid-state structure of [Fe(BDI)(OTf)] (**3**). Thermal ellipsoids are shown at the 30% probability level. Hydrogen atoms and cocrystallized solvent molecules are omitted for clarity. (B) Fourier transform of the transient nutation experiment of **3** (red trace) and that of the standard α,γ-bisdiphenylene-β-phenylallyl (BDPA; black trace). The inset shows the EPR spectrum of **3** and BDPA and the field position where the transient nutation experiment was done. (C) X-band EPR spectrum of **3** (2 mM) in a frozen acetonitrile solution at 10 K. (D) Zero-field ^{57}Fe Mössbauer spectrum (90 K) of **3** (blue trace, δ = 0.30 mm/s, $|\Delta E_Q|$ = 1.16 mm/s) and residual **2** (green trace). The red trace is the fitted Mössbauer spectrum.

electron is in a ligand-based orbital that antiferromagnetically couples to a metal-based d orbital with π-symmetry (S_{UCO} = 0.45; the overlap between the unrestricted corresponding orbitals (UCOs) is an indication of the strength of the coupling).[34] Both the Löwdin spin population (see SI) and the spin-density plots (Figure 4A) are consistent with the observed redox noninnocence of the ligand. Visual inspection shows that the spin density is primarily delocalized over the N1−C10−C12−N2 π framework, with the majority located on the C_{ipso}−C_{imine} carbon atoms, consistent with the contraction of the C10−C12 bond distance observed by X-ray crystallography (Table 1). In conclusion, the electronic structure of **3** is best described as an intermediate spin (S = 1) iron(II) metal center that is antiferromagnetically coupled to a ligand-based (S = 1/2) radical.

For the two-electron reduced species **4**, a different picture emerges. First, complex **4** was obtained by adding 2 equiv of Na(Hg) to a solution of **2** in acetonitrile (Figure 2A). The solid-state structure of **4** (Figure 7A) shows a neutral monometallic iron complex in a square-pyramidal geometry. A comparison of the bond lengths shows that while the C10−C12 distance remains fairly constant, the N1−C10 distance further elongates from 1.31(1) Å in **3** to 1.352(3) Å in **4**. The trend of gradual elongation of the N_{imine}−C_{imine} bond distance is consistent with data reported by Wieghardt et al.,[10d] Chirik et al.,[10a,b] and Uyeda and Zhou,[13a] who showed that in similar α-imino pyridine-based complexes almost all the one- and two-electron reductions are essentially ligand-based.

Like the previous case, several electronic configurations were evaluated using single-point calculations with the crystal structure coordinates of complex **4**. Overall, the singlet, triplet, quintet, BS(4,2), BS(3,1), BS (2,2), and BS(1,1) electronic configurations were evaluated. Our calculations indicate that the BS(2,2) solution is the ground state (see Supporting Information), which was further used for the full optimization of the structure. As shown in Table 1, the BS(2,2) solution reproduces the experimentally obtained bond metrics quite accurately and effectively describes complex **4** as an intermediate spin (S = 1) iron(II) metal center that antiferromagnetically couples to a ligand (S = 1) diradical. The presence of an intermediate spin (S = 1) iron(II) metal center is also evident from the zero-field ^{57}Fe Mössbauer parameters of **4** at 90 K (Figure 7B; δ = 0.26 mm/s; $|\Delta E_Q|$ = 0.79 mm/s), which are similar to other iron complexes having an intermediate spin.[10b,33]

The partial molecular orbital energy diagram of complex **4** (Figure 4B) shows that the two spin-up electrons are primarily located on the metal, in d orbitals that appear to be a mixture of yz and z^2. These interact magnetically with the spin-down electrons in two singly occupied ligand-based orbitals, with a spatial overlap of S_{UCO} = 0.50 and S_{UCO} = 0.58, respectively. The spin-density plot is consistent with the presence of two unpaired electrons on the metal center, with the rest of the electron density delocalized over the π-framework of the ligand (Figure 4B). We emphasize that the observed spin distribution is a feature of the BS calculation that is useful for providing a visual depiction of the distribution of unpaired electrons; it is

https://doi.org/10.1021/acs.inorgchem.1c02925
Inorg. Chem. 2021, 60, 18296−18306

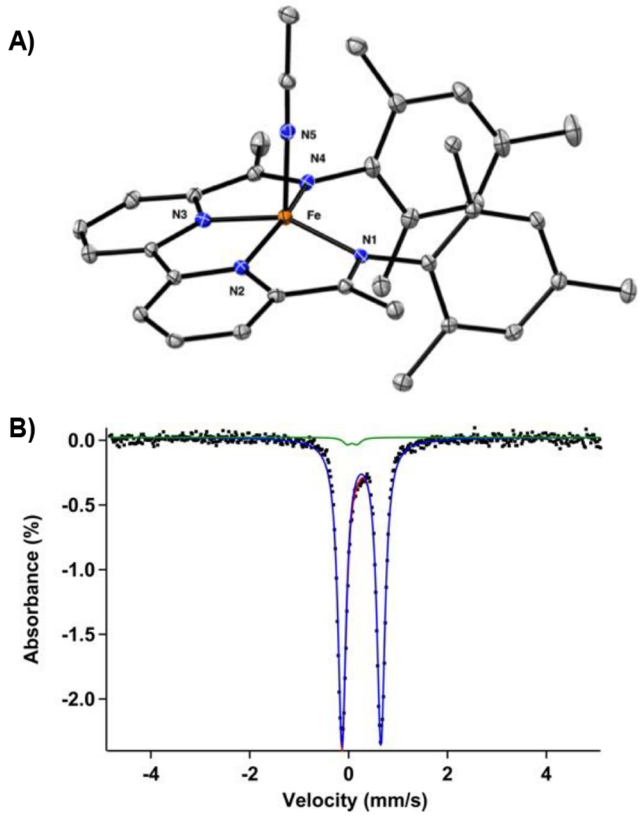

Figure 7. (A) Solid-state structure of the two-electron reduced complex [Fe(BDI)(MeCN)] (**4**). Thermal ellipsoids are shown at 30% probability. Hydrogen atoms and cocrystallized solvent molecules are omitted for clarity. (B) Zero-field ^{57}Fe Mössbauer spectrum (90 K) of **4** with an isomer shift value of δ = 0.26 mm/s and quadrupole splitting value of $|\Delta E_Q|$ = 0.79 mm/s.

not a real physical property of the complex. Overall, the multiplicity of the complex is a singlet, and it does not have spin-density. Notwithstanding, complex **4** is best described as an intermediate spin (S = 1) iron(II) metal center antiferromagnetically coupled to a ligand-based (S = 1) diradical giving an overall singlet ground state. Because of the singlet ground state, the complex is diamagnetic, yet its ^{1}H NMR and EPR spectra are uninformative and featureless, which is not uncommon for such species.[17]

The electronic description of the three-electron reduced complex **5** is potentially more complex. Because the reduction occurs at quite negative potentials, the final one-electron reduction could either be (i) metal based or (ii) ligand based, where a ligand-based reduction results in a trianionic ligand with significant radical character.[16]

The three-electron reduced complex **5** was obtained by treating a solution of **2** in THF with an excess of KC_8 (Figure 2A). Crystals of **5** were obtained by slow vapor diffusion of hexamethyldisiloxane into a concentrated solution of **5** in THF. The solid-state structure of **5** is shown in Figure 8 and features a square-planar iron complex with a potassium countercation coordinated by a crown-ether. Analyses of the bond metrics reveal further elongation of the N_{imine}−C_{imine} bond distances from 1.352(3) Å in **4** to 1.384(3) Å in **5** with a concomitant shortening of the C_{imine}−C_{ipso} distances from 1.419(3) Å in **4** to 1.389 Å in **5** (Table 1). It is important to note that the C10−N1 (1.384(2) Å) and the C10−C12

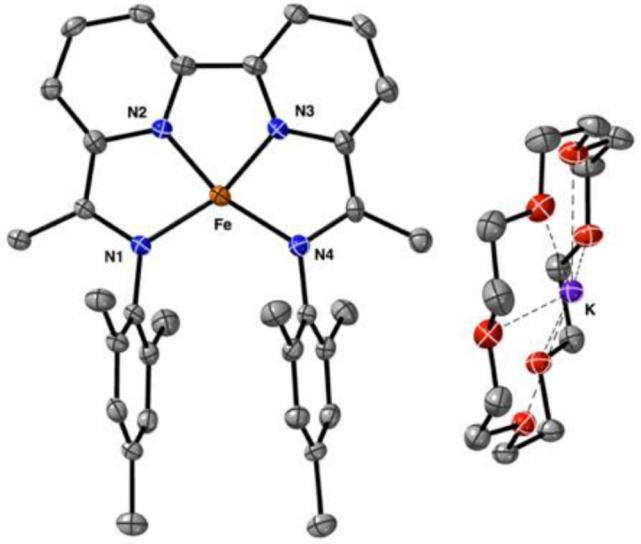

Figure 8. Solid-state structure of the three-electron reduced complex [Fe(BDI)][K(18-crown-6)$_2$] (**5**). Thermal ellipsoids are shown at 30% probability. Hydrogen atoms and cocrystallized solvent molecules are omitted for clarity.

(1.389(5) Å) bond distances in **5** are nearly identical, indicating almost complete delocalization of the radical. Furthermore, elongation of the bipyridine C12−N2 and C21−N3 bond distances from 1.345(4) and 1.347(4) Å in **2** to 1.404(5) and 1.401(5) Å in **5** suggest (partial) dearomatization of the bipyridine backbone, generating a trianionic ligand.[17] The structural parameters of **5** thus indicate another ligand-based reduction. Similar studies by Budzelaar and co-workers have shown that for structurally related PDI ligands, three electron reduction also leads to partial dearomatization of the pyridine backbone with an overall calculated doublet (S = 1/2) ground state of the ligand.[16]

A ligand-based reduction was also corroborated by the computational results. We evaluated the doublet, quartet, BS(4,3), BS(3,2), and BS(2,1) electronic configurations. The ground state was determined to be the BS(2,1) solution (see Supporting Information for further details), which corresponds to an intermediate spin (S = 1) iron metal center that is antiferromagnetically coupled to a ligand based (S = 1/2) radical. According to our calculations, the two unpaired electrons are essentially located in the metal's d_{xz} and d_{yz} orbitals, which is also evident from the spin-density plot (Figure 4C). One of these orbitals (d_{xz}) is magnetically coupled to a singly occupied orbital ligand-based orbital, with a relatively large spatial overlap (S_{UCO} = 0.56). Like complexes **3** and **4**, this radical is mainly delocalized over the N1−C10−C12−N2 π framework, resulting in partial dearomatization of the bipyridine ring. Furthermore, the BS(2,1) solution reproduces the experimentally determined bond metrics quite accurately (Table 1), corroborating the assignment of **5** as having an intermediate spin (S = 1) iron(II) metal center.

Overall, the BS(2,1) solution likely describes the electronic structure of **5** most accurately. However, the zero-field ^{57}Fe Mössbauer data of **5** at 90 K only partially agrees with such a conclusion, since two quadrupole doublets are consistently produced in a roughly 1:1 ratio (Figure S12). The first quadrupole doublet (δ = 0.47 mm/s; $|\Delta E_Q|$ = 0.37 mm/s) indeed suggests the presence of an intermediate spin iron(II) metal center and, therefore, implies a ligand based reduction.

https://doi.org/10.1021/acs.inorgchem.1c02925
Inorg. Chem. 2021, 60, 18296−18306

However, the second quadrupole doublet (δ = −0.12 mm/s; $|\Delta E_Q|$ = 0.38 mm/s) belongs to an unknown iron compound—possibly an Fe(I) species. Unfortunately, EPR spectroscopy was unable to further assist in elucidating the identity of this unknown species or assist in further elucidating the electronic structure of **5**, since no prominent features were observed in its EPR spectrum.[35]

SUMMARY AND CONCLUSIONS

We have demonstrated that monometallic complexes of the type [Fe(BDI)(OTf)$_2$] (**2**) can exist in five stable oxidation states. Crystallographic, spectroscopic, and computational studies have shown that the multiple redox events are characterized by extensive ligand-based reductions (BDI ⇄ BDI^{3-}), where the metal is only involved in redox processes M^{II} ⇄ M^{III}. The BDI ligand cycles between four oxidation states $[BDI]^0$ ⇄ $[BDI]^{3-}$, ultimately leading to partial dearomatization of the bipyridine backbone. For the final reduction event, a metal-based reduction seems to be plausible as well, but further studies are necessary. The computational studies also suggested the formation of a relatively rare intermediate spin (S = 1) penta-coordinated iron metal complex, which is in good agreement with the obtained zero-field ^{57}Fe Mössbauer spectra. Current studies are focused on utilizing the extensive redox noninnocence to facilitate potential catalytic reactions with earth-abundant metal complexes.

Computational Details. All structure optimizations and energy calculations were performed with ORCA 5.0.0[36] using the PBE0[37] functional and the def2-TZVP[38] basis set, with Grimme's D3[39] dispersion correction and Becke-Johnson damping.[40] Single-point energies to determine the correct electronic configuration of the ground state were performed using the crystal-structure coordinates. Broken-symmetry calculations were performed using the "BrokenSym" keyword and are reported in this text as BS(m,n), where the descriptor m refers to the number of spin-up electrons on one fragment and the descriptor n refers to the number of spin-down electrons on the second fragment ($m > n$). For each complex, the configuration identified as the ground state and the respective spin configuration were then used for full optimization from which relative energies were determined (see SI). Attempts to calculate other electronic configurations resulted either in higher energies or in undesired configurations and are detailed in the SI. Unrestricted corresponding orbitals[34] and their overlaps were calculated for the ground state broken-symmetry configuration. To calculate Mössbauer parameters, constrained optimizations using the TPSSh[41] functional with the TZVP[42] + CP(PPP)[43] basis sets were performed on the crystal-structure coordinates, in which the heavy atoms were kept frozen and the H atoms were allowed to optimize. Isomer shifts were calculated using coefficients reported by Römelt et al.[44] LOBA[25] calculations to obtain the Fe oxidation state were performed with Multiwfn 3.7.[45] Visualization of the orbitals and spin densities was done with PyMOL 1.7.4[46] based on cube files generated with orca_plot. Templates for all types of calculations are provided in the SI.

ASSOCIATED CONTENT

Supporting Information

The Supporting Information is available free of charge at https://pubs.acs.org/doi/10.1021/acs.inorgchem.1c02925.

Synthetic procedures, characterization data, computational details, and catalytic procedures (PDF)

Coordinate files (xyz format) for the optimized structures **2**−**5** (XYZ)

Accession Codes

CCDC 1908506, 1908509−1908510, 1962699−1962700, and 2030972 contain the supplementary crystallographic data for this paper. These data can be obtained free of charge via www.ccdc.cam.ac.uk/data_request/cif, or by emailing data_request@ccdc.cam.ac.uk, or by contacting The Cambridge Crystallographic Data Centre, 12 Union Road, Cambridge CB2 1EZ, UK; fax: +44 1223 336033.

AUTHOR INFORMATION

Corresponding Authors

Renana Gershoni-Poranne − *Laboratorium für Organische Chemie, ETH Zurich, Zurich 8093, Switzerland; Schulich Faculty of Chemistry, Technion − Israel Institute of Technology, Technion City 3200008 Haifa, Israel;* orcid.org/0000-0002-2233-6854; Email: rporanne@technion.ac.il

Graham de Ruiter − *Schulich Faculty of Chemistry, Technion − Israel Institute of Technology, Technion City 3200008 Haifa, Israel;* orcid.org/0000-0001-6008-286X; Email: graham@technion.ac.il

Authors

Ranjeesh Thenarukandiyil − *Schulich Faculty of Chemistry, Technion − Israel Institute of Technology, Technion City 3200008 Haifa, Israel*

Eno Paenurk − *Laboratorium für Organische Chemie, ETH Zurich, Zurich 8093, Switzerland;* orcid.org/0000-0002-6921-757X

Anthony Wong − *Department of Chemistry and Biochemistry, University of California, Santa Barbara, California 93106, United States;* orcid.org/0000-0001-6918-2437

Natalia Fridman − *Schulich Faculty of Chemistry, Technion − Israel Institute of Technology, Technion City 3200008 Haifa, Israel*

Amir Karton − *School of Molecular Science, The University of Western Australia, 6009 Perth, Australia;* orcid.org/0000-0002-7981-508X

Raanan Carmieli − *Department of Chemical Research Support, Weizmann Institute of Science, Rehovot 761000, Israel;* orcid.org/0000-0003-4418-916X

Gabriel Ménard − *Department of Chemistry and Biochemistry, University of California, Santa Barbara, California 93106, United States;* orcid.org/0000-0002-2801-0863

Complete contact information is available at: https://pubs.acs.org/10.1021/acs.inorgchem.1c02925

Notes

The authors declare no competing financial interest.

ACKNOWLEDGMENTS

This research was supported by the Azrieli Foundation and the Ministry of Energy under contract #219-11-130. G.d.R. is an Azrieli young faculty fellow and a Horev Fellow supported by the Taub Foundation. A.K. acknowledges an Australian Research Council (ARC) Future Fellowship (FT170100373). R.T. wishes to thank the Council for Higher Education in

Israel for an incoming PBC fellowship. R.G.P. is a Branco Weiss Fellow and a Career Advancement Fellow. R.G.P. and E.P. gratefully acknowledge the support of Prof. Peter Chen and of the ETH Zürich.

REFERENCES

(1) (a) Arevalo, R.; Chirik, P. J. Enabling Two-Electron Pathways with Iron and Cobalt: From Ligand Design to Catalytic Applications. *J. Am. Chem. Soc.* **2019**, *141*, 9106−9123. (b) Feichtner, K.-S.; Gessner, V. H. Cooperative Bond Activation Reactions with Carbene Complexes. *Chem. Commun.* **2018**, *54*, 6540−6553. (c) Khusnutdinova, J. R.; Milstein, D. Metal−Ligand Cooperation. *Angew. Chem., Int. Ed.* **2015**, *54*, 12236−12273. (d) Milstein, D. Metal−Ligand Cooperation by Aromatization−Dearomatization as a Tool in Single Bond Activation. *Philos. Trans. R. Soc., A* **2015**, *373*, 20140189. (e) Grützmacher, H. Cooperating Ligands in Catalysis. *Angew. Chem., Int. Ed.* **2008**, *47*, 1814−1818.

(2) (a) Chapovetsky, A.; Do, T. H.; Haiges, R.; Takase, M. K.; Marinescu, S. C. Proton-Assisted Reduction of CO_2 by Cobalt Aminopyridine Macrocycles. *J. Am. Chem. Soc.* **2016**, *138*, 5765−5768. (b) Umehara, K.; Kuwata, S.; Ikariya, T. N−N Bond Cleavage of Hydrazines with a Multiproton-Responsive Pincer-Type Iron Complex. *J. Am. Chem. Soc.* **2013**, *135*, 6754−6757. (c) Costentin, C.; Drouet, S.; Robert, M.; Savéant, J.-M. A Local Proton Source Enhances CO_2; Electroreduction to CO by a Molecular Fe Catalyst. *Science* **2012**, *338*, 90. (d) Hull, J. F.; Himeda, Y.; Wang, W.-H.; Hashiguchi, B.; Periana, R.; Szalda, D. J.; Muckerman, J. T.; Fujita, E. Reversible Hydrogen Storage Using CO_2 and a Proton-Switchable Iridium Catalyst in Aqueous Media under Mild Temperatures and Pressures. *Nat. Chem.* **2012**, *4*, 383. (e) Carver, C. T.; Matson, B. D.; Mayer, J. M. Electrocatalytic Oxygen Reduction by Iron Tetraarylporphyrins Bearing Pendant Proton Relays. *J. Am. Chem. Soc.* **2012**, *134*, 5444−5447. (f) Helm, M. L.; Stewart, M. P.; Bullock, R. M.; DuBois, M. R.; DuBois, D. L. A Synthetic Nickel Electrocatalyst with a Turnover Frequency Above 100,000 s^{-1}; for H_2 Production. *Science* **2011**, *333*, 863.

(3) (a) Rummelt, S. M.; Zhong, H.; Korobkov, I.; Chirik, P. J. Iron-Mediated Coupling of Carbon Dioxide and Ethylene: Macrocyclic Metallalactones Enable Access to Various Carboxylates. *J. Am. Chem. Soc.* **2018**, *140*, 11589−11593. (b) Broere, D. L. J.; Modder, D. K.; Blokker, E.; Siegler, M. A.; van der Vlugt, J. I. Metal−Metal Interactions in Heterobimetallic Complexes with Dinucleating Redox-Active Ligands. *Angew. Chem., Int. Ed.* **2016**, *55*, 2406−2410. (c) Lippert, C. A.; Arnstein, S. A.; Sherrill, C. D.; Soper, J. D. Redox-Active Ligands Facilitate Bimetallic O_2 Homolysis at Five-Coordinate Oxorhenium(V) Centers. *J. Am. Chem. Soc.* **2010**, *132*, 3879−3892. (d) Smith, A. L.; Hardcastle, K. I.; Soper, J. D. Redox-Active Ligand-Mediated Oxidative Addition and Reductive Elimination at Square Planar Cobalt(III): Multielectron Reactions for Cross-Coupling. *J. Am. Chem. Soc.* **2010**, *132*, 14358−14360. (e) Stanciu, C.; Jones, M. E.; Fanwick, P. E.; Abu-Omar, M. M. Multi-electron Activation of Dioxygen on Zirconium(IV) to Give an Unprecedented Bisperoxo Complex. *J. Am. Chem. Soc.* **2007**, *129*, 12400−12401.

(4) (a) Fujita, D.; Sugimoto, H.; Shiota, Y.; Morimoto, Y.; Yoshizawa, K.; Itoh, S. Catalytic C−H Amination Driven by Intramolecular Ligand-to-Nitrene One-Electron Transfer Through a Rhodium(iii) Centre. *Chem. Commun.* **2017**, *53*, 4849−4852. (b) Margulieux, G. W.; Bezdek, M. J.; Turner, Z. R.; Chirik, P. J. Ammonia Activation, H_2 Evolution and Nitride Formation from a Molybdenum Complex with a Chemically and Redox Noninnocent Ligand. *J. Am. Chem. Soc.* **2017**, *139*, 6110−6113. (c) Tutusaus, O.; Ni, C.; Szymczak, N. K. A Transition Metal Lewis Acid/Base Triad System for Cooperative Substrate Binding. *J. Am. Chem. Soc.* **2013**, *135*, 3403−3406. (d) Kraft, S. J.; Fanwick, P. E.; Bart, S. C. Carbon−Carbon Reductive Elimination from Homoleptic Uranium(IV) Alkyls Induced by Redox-Active Ligands. *J. Am. Chem. Soc.* **2012**, *134*, 6160−6168. (e) Nguyen, A. I.; Blackmore, K. J.; Carter, S. M.; Zarkesh, R. A.; Heyduk, A. F. One- and Two-Electron Reactivity of a Tantalum(V) Complex with a Redox-Active Tris(amido) Ligand. *J. Am. Chem. Soc.* **2009**, *131*, 3307−3316. (f) Ben-Ari, E.; Leitus, G.; Shimon, L. J. W.; Milstein, D. Metal−Ligand Cooperation in C−H and H_2 Activation by an Electron-Rich PNP Ir(I) System: Facile Ligand Dearomatization−Aromatization as Key Steps. *J. Am. Chem. Soc.* **2006**, *128*, 15390−15391.

(5) (a) Whittaker, J. W. The Radical Chemistry of Galactose Oxidase. *Arch. Biochem. Biophys.* **2005**, *433*, 227−239. (b) Denisov, I. G.; Makris, T. M.; Sligar, S. G.; Schlichting, I. Structure and Chemistry of Cytochrome P450. *Chem. Rev.* **2005**, *105*, 2253−2278.

(6) (a) Tezgerevska, T.; Alley, K. G.; Boskovic, C. Valence Tautomerism in Metal Complexes: Stimulated and Reversible Intramolecular Electron Transfer Between Metal Centers and Organic Ligands. *Coord. Chem. Rev.* **2014**, *268*, 23−40. (b) Luca, O. R.; Crabtree, R. H. Redox-Active Ligands in Catalysis. *Chem. Soc. Rev.* **2013**, *42*, 1440−1459. (c) Lyaskovskyy, V.; de Bruin, B. Redox Non-Innocent Ligands: Versatile New Tools to Control Catalytic Reactions. *ACS Catal.* **2012**, *2*, 270−279. (d) Praneeth, V. K. K.; Ringenberg, M. R.; Ward, T. R. Redox-Active Ligands in Catalysis. *Angew. Chem., Int. Ed.* **2012**, *51*, 10228−10234. (e) Storr, T.; Mukherjee, R. Preface for the Forum on Applications of Metal Complexes with Ligand-Centered Radicals. *Inorg. Chem.* **2018**, *57*, 9577−9579. (f) Chirik, P. J. Preface: Forum on Redox-Active Ligands. *Inorg. Chem.* **2011**, *50*, 9737−9740.

(7) Chirik, P. J.; Wieghardt, K. Radical Ligands Confer Nobility on Base-Metal Catalysts. *Science* **2010**, *327*, 794.

(8) (a) Eisenberg, R.; Gray, H. B. Noninnocence in Metal Complexes: A Dithiolene Dawn. *Inorg. Chem.* **2011**, *50*, 9741−9751. (b) Stiefel, E. I.; Eisenberg, R.; Rosenberg, R. C.; Gray, H. B. Characterization and Electronic Structures of Six-Coordinate Trigonal-Prismatic Complexes. *J. Am. Chem. Soc.* **1966**, *88*, 2956−2966.

(9) (a) Broere, D. L. J.; Mercado, B. Q.; Lukens, J. T.; Vilbert, A. C.; Banerjee, G.; Lant, H. M. C.; Lee, S. H.; Bill, E.; Sproules, S.; Lancaster, K. M.; Holland, P. L. Reversible Ligand-Centered Reduction in Low-Coordinate Iron Formazanate Complexes. *Chem. - Eur. J.* **2018**, *24*, 9417−9425. (b) Henthorn, J. T.; Agapie, T. Modulation of Proton-Coupled Electron Transfer through Molybdenum−Quinonoid Interactions. *Inorg. Chem.* **2016**, *55*, 5337−5342. (c) Ray, K.; Petrenko, T.; Wieghardt, K.; Neese, F. Joint Spectroscopic and Theoretical Investigations of Transition Metal Complexes Involving Non-Innocent Ligands. *Dalton Trans.* **2007**, 1552−1566. (d) Kapre, R. R.; Bothe, E.; Weyhermüller, T.; DeBeer George, S.; Wieghardt, K. Electronic Structure of Neutral and Monoanionic Tris(benzene-1,2-dithiolato)metal Complexes of Molybdenum and Tungsten. *Inorg. Chem.* **2007**, *46*, 5642−5650. (e) Chłopek, K.; Bothe, E.; Neese, F.; Weyhermüller, T.; Wieghardt, K. Molecular and Electronic Structures of Tetrahedral Complexes of Nickel and Cobalt Containing N,N′-Disubstituted, Bulky o-Diiminobenzosemiquinonate(1−) π-Radical Ligands. *Inorg. Chem.* **2006**, *45*, 6298−6307. (f) Herebian, D.; Bothe, E.; Neese, F.; Weyhermüller, T.; Wieghardt, K. Molecular and Electronic Structures of Bis-(o-diiminobenzosemiquinonato)metal(II) Complexes (Ni, Pd, Pt), Their Monocations and -Anions, and of Dimeric Dications Containing Weak Metal−Metal Bonds. *J. Am. Chem. Soc.* **2003**, *125*, 9116−9128. (g) Harris, C. F.; Bayless, M. B.; van Leest, N. P.; Bruch, Q. J.; Livesay, B. N.; Bacsa, J.; Hardcastle, K. I.; Shores, M. P.; de Bruin, B.; Soper, J. D. Redox-Active Bis(phenolate) N-Heterocyclic Carbene [OCO] Pincer Ligands Support Cobalt Electron Transfer Series Spanning Four Oxidation States. *Inorg. Chem.* **2017**, *56*, 12421−12435. (h) Lu, C. C.; Bill, E.; Weyhermüller, T.; Bothe, E.; Wieghardt, K. The Monoanionic π-Radical Redox State of α-Iminoketones in Bis(ligand)metal Complexes of Nickel and Cobalt. *Inorg. Chem.* **2007**, *46*, 7880−7889. (i) Khusniyarov, M. M.; Harms, K.; Burghaus, O.; Sundermeyer, J. Molecular and Electronic Structures of Homoleptic Nickel and Cobalt Complexes with Non-Innocent Bulky Diimine Ligands Derived from Fluorinated 1,4-Diaza-1,3-butadiene (DAD) and Bis(arylimino)acenaphthene (BIAN). *Eur.*

https://doi.org/10.1021/acs.inorgchem.1c02925
Inorg. Chem. 2021, 60, 18296−18306

J. Inorg. Chem. **2006**, *2006*, 2985−2996. (j) Chaudhuri, P.; Verani, C. N.; Bill, E.; Bothe, E.; Weyhermüller, T.; Wieghardt, K. Electronic Structure of Bis(o-iminobenzosemiquinonato)metal Complexes (Cu, Ni, Pd). The Art of Establishing Physical Oxidation States in Transition-Metal Complexes Containing Radical Ligands. *J. Am. Chem. Soc.* **2001**, *123*, 2213−2223.

(10) (a) Bowman, A. C.; Milsmann, C.; Hojilla Atienza, C. C.; Lobkovsky, E.; Wieghardt, K.; Chirik, P. J. Synthesis and Molecular and Electronic Structures of Reduced Bis(imino)pyridine Cobalt Dinitrogen Complexes: Ligand versus Metal Reduction. *J. Am. Chem. Soc.* **2010**, *132*, 1676−1684. (b) Bart, S. C.; Chłopek, K.; Bill, E.; Bouwkamp, M. W.; Lobkovsky, E.; Neese, F.; Wieghardt, K.; Chirik, P. J. Electronic Structure of Bis(imino)pyridine Iron Dichloride, Monochloride, and Neutral Ligand Complexes: A Combined Structural, Spectroscopic, and Computational Study. *J. Am. Chem. Soc.* **2006**, *128*, 13901−13912. (c) Budzelaar, P. H. M.; de Bruin, B.; Gal, A. W.; Wieghardt, K.; van Lenthe, J. H. Metal-to-Ligand Electron Transfer in Diiminopyridine Complexes of Mn−Zn. A Theoretical Study. *Inorg. Chem.* **2001**, *40*, 4649−4655. (d) de Bruin, B.; Bill, E.; Bothe, E.; Weyhermüller, T.; Wieghardt, K. Molecular and Electronic Structures of Bis(pyridine-2,6-diimine)metal Complexes $[ML_2](PF_6)_n$ (n = 0, 1, 2, 3; M = Mn, Fe, Co, Ni, Cu, Zn). *Inorg. Chem.* **2000**, *39*, 2936−2947. (e) Lu, C. C.; Bill, E.; Weyhermüller, T.; Bothe, E.; Wieghardt, K. Neutral Bis(α-iminopyridine)metal Complexes of the First-Row Transition Ions (Cr, Mn, Fe, Co, Ni, Zn) and Their Monocationic Analogues: Mixed Valency Involving a Redox Noninnocent Ligand System. *J. Am. Chem. Soc.* **2008**, *130*, 3181−3197. (f) Lu, C. C.; Weyhermüller, T.; Bill, E.; Wieghardt, K. Accessing the Different Redox States of α-Iminopyridines within Cobalt Complexes. *Inorg. Chem.* **2009**, *48*, 6055−6064.

(11) (a) Hoyt, J. M.; Schmidt, V. A.; Tondreau, A. M.; Chirik, P. J. Iron Catalyzed Intermolecular [2 + 2] Cycloadditions of Unactivated Alkenes. *Science* **2015**, *349*, 960. (b) Tondreau, A. M.; Atienza, C. C. H.; Weller, K. J.; Nye, S. A.; Lewis, K. M.; Delis, J. G. P.; Chirik, P. J. Iron Catalysts for Selective Anti-Markovnikov Alkene Hydrosilylation Using Tertiary Silanes. *Science* **2012**, *335*, 567. (c) Darmon, J. M.; Stieber, S. C. E.; Sylvester, K. T.; Fernández, I.; Lobkovsky, E.; Semproni, S. P.; Bill, E.; Wieghardt, K.; DeBeer, S.; Chirik, P. J. Oxidative Addition of Carbon−Carbon Bonds with a Redox-Active Bis(imino)pyridine Iron Complex. *J. Am. Chem. Soc.* **2012**, *134*, 17125−17137.

(12) (a) Werth, J.; Uyeda, C. Cobalt-Catalyzed Reductive Dimethylcyclopropanation of 1,3-Dienes. *Angew. Chem., Int. Ed.* **2018**, *57*, 13902−13906. (b) Krautwald, S.; Bezdek, M. J.; Chirik, P. J. Cobalt-Catalyzed 1,1-Diboration of Terminal Alkynes: Scope, Mechanism, and Synthetic Applications. *J. Am. Chem. Soc.* **2017**, *139*, 3868−3875. (c) Obligacion, J. V.; Bezdek, M. J.; Chirik, P. J. C(sp2)-H Borylation of fluorinated arenes using an air-stable cobalt precatalyst: electronically enhanced site selectivity enables synthetic opportunities. *J. Am. Chem. Soc.* **2017**, *139*, 2825−2832. (d) Friedfeld, M. R.; Shevlin, M.; Margulieux, G. W.; Campeau, L.-C.; Chirik, P. J. Cobalt-Catalyzed Enantioselective Hydrogenation of Minimally Functionalized Alkenes: Isotopic Labeling Provides Insight into the Origin of Stereoselectivity and Alkene Insertion Preferences. *J. Am. Chem. Soc.* **2016**, *138*, 3314−3324. (e) Obligacion, J. V.; Chirik, P. J. Bis(imino)pyridine Cobalt-Catalyzed Alkene Isomerization-Hydroboration: A Strategy for Remote Hydrofunctionalization with Terminal Selectivity. *J. Am. Chem. Soc.* **2013**, *135*, 19107−19110.

(13) (a) Zhou, Y.-Y.; Uyeda, C. Catalytic reductive [4 + 1]-cycloadditions of vinylidenes and dienes. *Science* **2019**, *363*, 857. (b) Zhou, Y.-Y.; Hartline, D. R.; Steiman, T. J.; Fanwick, P. E.; Uyeda, C. Dinuclear Nickel Complexes in Five States of Oxidation Using a Redox-Active Ligand. *Inorg. Chem.* **2014**, *53*, 11770−11777. (c) Powers, I. G.; Andjaba, J. M.; Luo, X.; Mei, J.; Uyeda, C. Catalytic Azoarene Synthesis from Aryl Azides Enabled by a Dinuclear Ni Complex. *J. Am. Chem. Soc.* **2018**, *140*, 4110−4118. (d) Pal, S.; Uyeda, C. Evaluating the Effect of Catalyst Nuclearity in Ni-Catalyzed Alkyne Cyclotrimerizations. *J. Am. Chem. Soc.* **2015**, *137*, 8042−8045. (e) Pappas, I.; Treacy, S.; Chirik, P. J. Alkene Hydrosilylation Using Tertiary Silanes with α-Diimine Nickel Catalysts. Redox-Active Ligands Promote a Distinct Mechanistic Pathway from Platinum Catalysts. *ACS Catal.* **2016**, *6*, 4105−4109.

(14) Carney, J. R.; Dillon, B. R.; Campbell, L.; Thomas, S. P. Manganese-Catalyzed Hydrofunctionalization of Alkenes. *Angew. Chem., Int. Ed.* **2018**, *57*, 10620−10624.

(15) (a) Flisak, Z.; Sun, W.-H. Progression of Diiminopyridines: From Single Application to Catalytic Versatility. *ACS Catal.* **2015**, *5*, 4713−4724. (b) Mashima, K. Redox-active α-Diimine Complexes of Early Transition Metals: From Bonding to Catalysis. *Bull. Chem. Soc. Jpn.* **2020**, *93*, 799. (c) Chirik, P. J. Iron- and Cobalt-Catalyzed Alkene Hydrogenation: Catalysis with Both Redox-Active and Strong Field Ligands. *Acc. Chem. Res.* **2015**, *48*, 1687−1695.

(16) Enright, D.; Gambarotta, S.; Yap, G. P. A.; Budzelaar, P. H. M. The Ability of the α,α′-Diiminopyridine Ligand System to Accept Negative Charge: Isolation of Paramagnetic and Diamagnetic Trianions. *Angew. Chem., Int. Ed.* **2002**, *41*, 3873−3876.

(17) Tondreau, A. M.; Stieber, S. C. E.; Milsmann, C.; Lobkovsky, E.; Weyhermüller, T.; Semproni, S. P.; Chirik, P. J. Oxidation and Reduction of Bis(imino)pyridine Iron Dinitrogen Complexes: Evidence for Formation of a Chelate Trianion. *Inorg. Chem.* **2013**, *52*, 635−646.

(18) Bowman, A. C.; Sproules, S.; Wieghardt, K. Electronic Structures of the $[V(tbpy)_3]^z$ (z = 3+, 2+, 0, 1−) Electron Transfer Series. *Inorg. Chem.* **2012**, *51*, 3707−3717.

(19) (a) Small, B. L.; Brookhart, M.; Bennett, A. M. A. Highly Active Iron and Cobalt Catalysts for the Polymerization of Ethylene. *J. Am. Chem. Soc.* **1998**, *120*, 4049−4050. (b) Britovsek, G. J. P.; Gibson, V. C.; McTavish, S. J.; Solan, G. A.; White, A. J. P.; Williams, D. J.; Britovsek, G. J. P.; Kimberley, B. S.; Maddox, P. J. Novel olefin polymerization catalysts based on iron and cobalt. *Chem. Commun.* **1998**, 849−850.

(20) Chirik, P. J. Electronic Structures of Reduced Manganese, Iron, and Cobalt Complexes Bearing Redox-Active Bis(imino)pyridine Pincer Ligands. In *Pincer and Pincer-Type Complexes: Applications in Organic Synthesis and Catalysis*; Szabo, K. J.; Wendt, O. F., Eds.; Wiley-VCH: Weinheim, Germany, 2014; pp 189−212.

(21) (a) Ueda, Y.; Tsurugi, H.; Mashima, K. Cobalt-Catalyzed E-Selective Cross-Dimerization of Terminal Alkynes: A Mechanism Involving Cobalt(0/II) Redox Cycles. *Angew. Chem., Int. Ed.* **2020**, *59*, 1552−1556. (b) Hu, M.-Y.; Lian, J.; Sun, W.; Qiao, T.-Z.; Zhu, S.-F. Iron-catalyzed dihydrosilylation of alkynes: Efficient access to geminal bis(silanes). *J. Am. Chem. Soc.* **2019**, *141*, 4579−4583. (c) Kobayashi, K.; Taguchi, D.; Moriuchi, T.; Nakazawa, H. Chemoselective Hydrosilylation of Olefin/Ketone Catalyzed by Iminobipyridine Fe and Co complexes. *ChemCatChem* **2020**, *12*, 736−739. (d) Huang, Q.; Hu, M.-Y.; Zhu, S.-F. Cobalt-Catalyzed Cyclization/Hydroboration of 1,6-Diynes with Pinacolborane. *Org. Lett.* **2019**, *21*, 7883−7887. (e) Kobayashi, K.; Teratani, S.; Izumori, Y.; Hayasaka, K.; Nakazawa, H. Hydrosilylation of diene derivatives catalyzed by Fe-iminobipyridine complexes aiming at syntheses of organosilane compounds containing a terminal olefin portion. *Bull. Chem. Soc. Jpn.* **2019**, *92*, 105−114. (f) Kobayashi, K.; Izumori, Y.; Taguchi, D.; Nakazawa, H. Hydrosilylation of ketones catalyzed by iron iminobipyridine complexes and accelerated by Lewis bases. *ChemPlusChem* **2019**, *84*, 1094−1102. (g) Ueda, Y.; Tsujimoto, N.; Yurino, T.; Tsurugi, H.; Mashima, K. Nickel-catalyzed cyanation of aryl halides and triflates using acetonitrile via C−CN bond cleavage assisted by 1,4-bis(trimethylsilyl)-2,3,5,6-tetramethyl-1,4-dihydropyrazine. *Chem. Sci.* **2019**, *10*, 994−999. (h) Hu, M.-Y.; He, Q.; Fan, S.-J.; Wang, Z.-C.; Liu, L.-Y.; Mu, Y.-J.; Peng, Q.; Zhu, S.-F. Ligands with 1,10-phenanthroline scaffold for highly regioselective iron-catalyzed alkene hydrosilylation. *Nat. Commun.* **2018**, *9*, 221. (i) Toya, Y.; Hayasaka, K.; Nakazawa, H. Hydrosilylation of Olefins Catalyzed by Iron Complexes Bearing Ketimine-Type Iminobipyridine Ligands. *Organometallics* **2017**, *36*, 1727−1735. (j) Zell, T.; Milko, P.; Fillman, K. L.; Diskin-Posner, Y.; Bendikov, T.; Iron, M. A.; Leitus, G.; Ben-David, Y.; Neidig, M. L.; Milstein, D. Iron Dicarbonyl Complexes Featuring Bipyridine-Based PNN Pincer Ligands with Short

https://doi.org/10.1021/acs.inorgchem.1c02925
Inorg. Chem. 2021, 60, 18296−18306

Interpyridine C−C Bond Lengths: Innocent or Non-Innocent Ligand? *Chem. - Eur. J.* **2014**, *20*, 4403−4413. (k) Zhang, L.; Zuo, Z.; Leng, X.; Huang, Z. A Cobalt-Catalyzed Alkene Hydroboration with Pinacolborane. *Angew. Chem., Int. Ed.* **2014**, *53*, 2696−2700.
(22) Berka, L. H.; Gagne, R. R.; Philippon, G. E.; Wheeler, C. E. Transition Metal Complexes of 1,10-Phenanthroline and 2,2′-Bipyridine. *Inorg. Chem.* **1970**, *9*, 2705−2709.
(23) Krejčik, M.; Vlček, A. A. Electrochemical Formation of Dianions of 2,2′-Bipyridine and Related Compounds. *J. Electroanal. Chem. Interfacial Electrochem.* **1991**, *313*, 243−257.
(24) Griffith, G. A.; Al-Khatib, M. J.; Patel, K.; Singh, K.; Solan, G. A. Solid and Solution State Flexibility of Sterically Congested Bis(imino)bipyridine Complexes of Zinc(ii) and Nickel(ii). *Dalton Trans.* **2009**, 185−196.
(25) Thom, A. J. W.; Sundstrom, E. J.; Head-Gordon, M. LOBA: a localized orbital bonding analysis to calculate oxidation states, with application to a model water oxidation catalyst. *Phys. Chem. Chem. Phys.* **2009**, *11*, 11297−11304.
(26) (a) Wang, M.; England, J.; Weyhermüller, T.; Wieghardt, K. Molecular and Electronic Structures of the Members of the Electron Transfer Series $[Mn(bpy)_3]^n$ (n = 2+, 1+, 0, 1−) and $[Mn(tpy)_2]^m$ (m = 4+, 3+, 2+, 1+, 0). An Experimental and Density Functional Theory Study. *Inorg. Chem.* **2014**, *53*, 2276−2287. (b) England, J.; Scarborough, C. C.; Weyhermüller, T.; Sproules, S.; Wieghardt, K. Electronic Structures of the Electron Transfer Series [M(bpy)3]n, $[M(tpy)_2]^n$, and $[Fe(tbpy)_3]^n$ (M = Fe, Ru; n = 3+, 2+, 1+, 0, 1−): A Mössbauer Spectroscopic and DFT Study. *Eur. J. Inorg. Chem.* **2012**, *2012*, 4605−4621. (c) Scarborough, C. C.; Lancaster, K. M.; DeBeer, S.; Weyhermüller, T.; Sproules, S.; Wieghardt, K. Experimental Fingerprints for Redox-Active Terpyridine in $[Cr(tpy)_2](PF_6)_n$ (n = 3−0), and the Remarkable Electronic Structure of $[Cr(tpy)_2]^{1-}$. *Inorg. Chem.* **2012**, *51*, 3718−3732. (d) Scarborough, C. C.; Sproules, S.; Weyhermüller, T.; DeBeer, S.; Wieghardt, K. Electronic and Molecular Structures of the Members of the Electron Transfer Series $[Cr(tbpy)_3]^n$ (n = 3+, 2+, 1+, 0): An X-ray Absorption Spectroscopic and Density Functional Theoretical Study. *Inorg. Chem.* **2011**, *50*, 12446−12462.
(27) (a) Sproules, S.; Weyhermüller, T.; DeBeer, S.; Wieghardt, K. Six-Membered Electron Transfer Series $[V(dithiolene)_3]^z$ (z = 1+, 0, 1−, 2−, 3−, 4−). An X-ray Absorption Spectroscopic and Density Functional Theoretical Study. *Inorg. Chem.* **2010**, *49*, 5241−5261. (b) Wharton, E. J.; McCleverty, J. A. Transition-Metal Dithiolenes. Part VIII. Metal Complexes of Tris-Tetrachlorobenzene-1,2-dithiol and Related Compounds. *J. Chem. Soc. A* **1969**, 2258−2266. (c) Eisenberg, R.; Stiefel, E. I.; Rosenberg, R. C.; Gray, H. B. Six-Coordinate Trigonal-Prismatic Complexes of First-Row Transition Metals1. *J. Am. Chem. Soc.* **1966**, *88*, 2874−2876. (d) Davison, A.; Edelstein, N.; Holm, R. H.; Maki, A. H. Synthetic and Paramagnetic Resonance Studies of Trigonal Vanadium Complexes. *Inorg. Chem.* **1965**, *4*, 55−59.
(28) Surawatanawong, P.; Sproules, S.; Neese, F.; Wieghardt, K. Electronic Structures and Spectroscopy of the Electron Transfer Series $[Fe(NO)L_2]^z$ (z = 1+, 0, 1−, 2−,3−; L = Dithiolene). *Inorg. Chem.* **2011**, *50*, 12064−12074.
(29) (a) Hunt, C.; Peterson, M.; Anderson, C.; Chang, T.; Wu, G.; Scheiner, S.; Ménard, G. Switchable Aromaticity in an Isostructural Mn Phthalocyanine Series Isolated in Five Separate Redox States. *J. Am. Chem. Soc.* **2019**, *141*, 2604−2613. (b) Honda, T.; Kojima, T.; Fukuzumi, S. Proton-Coupled Electron-Transfer Reduction of Dioxygen Catalyzed by a Saddle-Distorted Cobalt Phthalocyanine. *J. Am. Chem. Soc.* **2012**, *134*, 4196−4206. (c) Lansky, D. E.; Mandimutsira, B.; Ramdhanie, B.; Clausén, M.; Penner-Hahn, J.; Zvyagin, S. A.; Telser, J.; Krzystek, J.; Zhan, R.; Ou, Z.; Kadish, K. M.; Zakharov, L.; Rheingold, A. L.; Goldberg, D. P. Synthesis, Characterization, and Physicochemical Properties of Manganese(III) and Manganese(V)−Oxo Corrolazines. *Inorg. Chem.* **2005**, *44*, 4485−4498.
(30) (a) Bruch, Q. J.; Lindley, B. M.; Askevold, B.; Schneider, S.; Miller, A. J. M. A Ruthenium Hydrido Dinitrogen Core Conserved across Multielectron/Multiproton Changes to the Pincer Ligand Backbone. *Inorg. Chem.* **2018**, *57*, 1964−1975. (b) Zhou, W.; Thompson, J. R.; Leznoff, C. C.; Leznoff, D. B. The Redox-Active Chromium Phthalocyanine System: Isolation of Five Oxidation States from Pc4−CrI to Pc2−CrIII. *Chem. - Eur. J.* **2017**, *23*, 2323−2331. (c) Buss, J. A.; Agapie, T. Four-Electron Deoxygenative Reductive Coupling of Carbon Monoxide at a Single Metal Site. *Nature* **2016**, *529*, 72. (d) Kokatam, S.; Weyhermüller, T.; Bothe, E.; Chaudhuri, P.; Wieghardt, K. Structural Characterization of Four Members of the Electron-Transfer Series $[PdII(L)_2)_2]^n$ (L = o-Iminophenolate Derivative; n = 2−, 1−, 0, 1+, 2+). Ligand Mixed Valency in the Monocation and Monoanion with S = 1/2 Ground States. *Inorg. Chem.* **2005**, *44*, 3709−3717. (e) Backes-Dahmann, G.; Herrmann, W.; Wieghardt, K.; Weiss, J. Preparation and Electrochemical Investigation of Monomeric Complexes of Molybdenum(0-VI) with the Ligand 1,4,7-trimethyl-1,4,7-triazacyclononane (L). Crystal Structure of $[Mo^{IV}LBr_3](PF_6)$. *Inorg. Chem.* **1985**, *24*, 485−491.
(31) Seperate studies reported by Chirik and co-workes indicate that pyridine diimine (PDI) complexes of iron can also exist in more than four oxidation states, see: (i) Tondreau, A. M.; Stieber, S. C. E.; Milsmann, C.; Lobkovsky, E.; Weyhermuller, T.; Semproni, S. P.; Chirik, P. J. Oxidation and Reduction of Bis(imino)pyridine Iron Dinitrogen Complexes: Evidence for Formation of a Chelate Trianion. *Inorg. Chem.* **2013**, *52*, 635−646. (ii) Bart, S. C.; Chłopek, K.; Bill, E.; Bouwkamp, M. W.; Lobkovsky, E.; Neese, F.; Wieghardt, K.; Chirik, P. J. *J. Am. Chem. Soc.* **2006**, *128*, 13901−13912.
(32) Astashkin, A. V.; Schweiger, A. Electron-spin transient nutation: a new approach to simplify the interpretation of ESR spectra. *Chem. Phys. Lett.* **1990**, *174*, 595−602.
(33) Ray, K.; Begum, A.; Weyhermüller, T.; Piligkos, S.; van Slageren, J.; Neese, F.; Wieghardt, K. The Electronic Structure of the Isoelectronic, Square-Planar Complexes [FeII(L)2]2- and [CoIII-(LBu)2]- (L2- and (LBu)2- = Benzene-1,2-dithiolates): An Experimental and Density Functional Theoretical Study. *J. Am. Chem. Soc.* **2005**, *127*, 4403−4415.
(34) (a) Neese, F. Definition of corresponding orbitals and the diradical character in broken symmetry DFT calculations on spin coupled systems. *J. Phys. Chem. Solids* **2004**, *65*, 781−785. (b) Neese, F. Prediction of molecular properties and molecular spectroscopy with density functional theory: From fundamental theory to exchange-coupling. *Coord. Chem. Rev.* **2009**, *253*, 526−563.
(35) Taiwo, F. A. Electron paramagnetic resonance spectroscopic studies of iron and copper proteins. *Spectroscopy* **2003**, *17*, 53−63.
(36) (a) Neese, F. The ORCA program system. *Wiley Interdiscip. Rev.: Comput. Mol. Sci.* **2012**, *2*, 73−78. (b) Neese, F. Software update: the ORCA program system, version 4.0. *Wiley Interdiscip. Rev.: Comput. Mol. Sci.* **2018**, *8*, e1327. (c) Neese, F.; Wennmohs, F.; Becker, U.; Riplinger, C. The ORCA quantum chemistry program package. *J. Chem. Phys.* **2020**, *152*, 224108.
(37) (a) Perdew, J. P.; Burke, K.; Ernzerhof, M. Generalized Gradient Approximation Made Simple. *Phys. Rev. Lett.* **1996**, *77*, 3865−3868. (b) Ernzerhof, M.; Scuseria, G. E. Assessment of the Perdew−Burke−Ernzerhof exchange-correlation functional. *J. Chem. Phys.* **1999**, *110*, 5029−5036. (c) Adamo, C.; Barone, V. Toward reliable density functional methods without adjustable parameters: The PBE0 model. *J. Chem. Phys.* **1999**, *110*, 6158−6170.
(38) Weigend, F.; Ahlrichs, R. Balanced basis sets of split valence, triple zeta valence and quadruple zeta valence quality for H to Rn: Design and assessment of accuracy. *Phys. Chem. Chem. Phys.* **2005**, *7*, 3297−3305.
(39) Grimme, S.; Antony, J.; Ehrlich, S.; Krieg, H. A consistent and accurate ab initio parametrization of density functional dispersion correction (DFT-D) for the 94 elements H-Pu. *J. Chem. Phys.* **2010**, *132*, 154104.
(40) (a) Johnson, E. R.; Becke, A. D. A post-Hartree−Fock model of intermolecular interactions. *J. Chem. Phys.* **2005**, *123*, 024101. (b) Grimme, S.; Ehrlich, S.; Goerigk, L. Effect of the damping

https://doi.org/10.1021/acs.inorgchem.1c02925
Inorg. Chem. 2021, 60, 18296−18306

function in dispersion corrected density functional theory. *J. Comput. Chem.* **2011**, *32*, 1456−1465.
(41) (a) Tao, J.; Perdew, J. P.; Staroverov, V. N.; Scuseria, G. E. Climbing the Density Functional Ladder: Nonempirical Meta–Generalized Gradient Approximation Designed for Molecules and Solids. *Phys. Rev. Lett.* **2003**, *91*, 146401. (b) Staroverov, V. N.; Scuseria, G. E.; Tao, J.; Perdew, J. P. Comparative assessment of a new nonempirical density functional: Molecules and hydrogen-bonded complexes. *J. Chem. Phys.* **2003**, *119*, 12129−12137.
(42) Peintinger, M. F.; Oliveira, D. V.; Bredow, T. Consistent Gaussian basis sets of triple-zeta valence with polarization quality for solid-state calculations. *J. Comput. Chem.* **2013**, *34*, 451−459.
(43) Neese, F. Prediction and interpretation of the 57Fe isomer shift in Mössbauer spectra by density functional theory. *Inorg. Chim. Acta* **2002**, *337*, 181−192.
(44) Römelt, M.; Ye, S.; Neese, F. Calibration of Modern Density Functional Theory Methods for the Prediction of 57Fe Mössbauer Isomer Shifts: Meta-GGA and Double-Hybrid Functionals. *Inorg. Chem.* **2009**, *48*, 784−785.
(45) Lu, T.; Chen, F. Multiwfn: A multifunctional wavefunction analyzer. *J. Comput. Chem.* **2012**, *33*, 580−592.
(46) *The PyMOL Molecular Graphics System*; Schrödinger, LLC, 2014.

https://doi.org/10.1021/acs.inorgchem.1c02925
Inorg. Chem. 2021, 60, 18296−18306